Accepted Manuscript

An advanced underplatform damper modelling approach based on a microslip contact model

L. Pesaresi, J. Armand, C.W. Schwingshackl, L. Salles, C. Wong

PII: S0022-460X(18)30520-0

DOI: 10.1016/j.jsv.2018.08.014

Reference: YJSVI 14305

To appear in: *Journal of Sound and Vibration*

Received Date: 18 April 2018

Revised Date: 27 July 2018

Accepted Date: 10 August 2018

Please cite this article as: L. Pesaresi, J. Armand, C.W. Schwingshackl, L. Salles, C. Wong, An advanced underplatform damper modelling approach based on a microslip contact model, *Journal of Sound and Vibration* (2018), doi: 10.1016/j.jsv.2018.08.014.

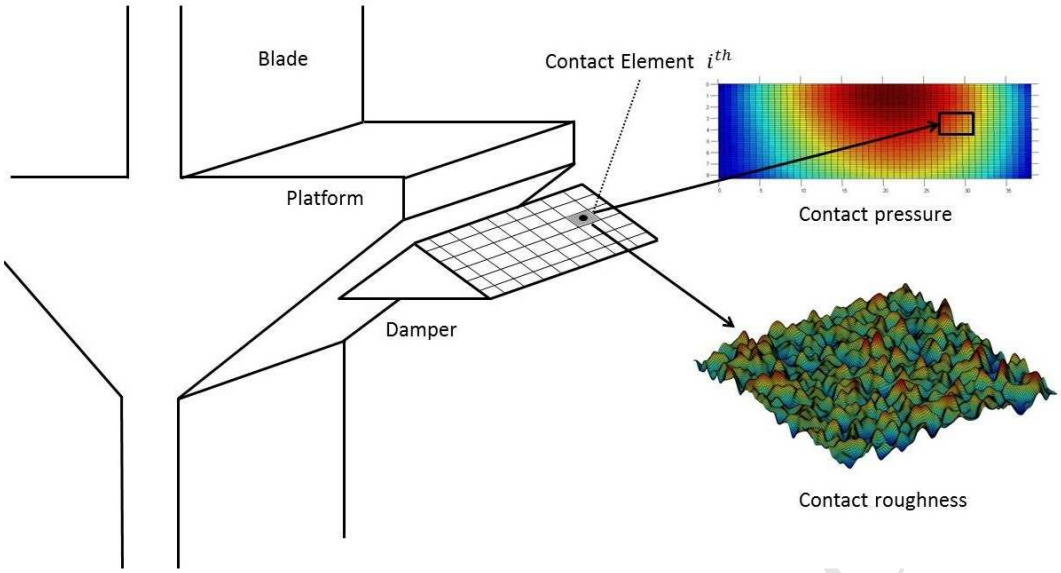

An advanced underplatform damper modelling approach based on a microslip contact model

L.Pesaresi[a,*], J.Armand[a], C.W.Schwingshackl[a], L.Salles[a], C.Wong[b]

[a]*Imperial College London, London SW7 2AZ, UK*
[b]*Rolls-Royce plc, Derby DE2 48J, UK*

Abstract

High-cycle fatigue caused by large resonance stresses remains one of the most common causes of turbine blade failures. Friction dampers are one of the most effective and practical solutions to limit the vibration amplitudes, and shift the resonance frequencies of the turbine assemblies far from operating speeds. However, predicting the effects of underplatform dampers on the dynamics of the blades with good accuracy still represents a major challenge today, due to the complex nature of the nonlinear forces at the interface, characterised by transitions between stick, slip, and separation conditions. The most common modelling approaches developed recently are based on the explicit FE model for the damper, and on a dense grid of 3D contact elements comprised of Jenkins elements, or on a single 2D microslip element on each surface. In this paper, a combination of the two approaches is proposed. A 3D microslip element, based on a modified Valanis model is proposed and a series of these elements are used to describe the contact interface. This new approach allows to implicitly account for the microscale energy dissipation as well as the pressure-dependent contact stiffness caused by the roughness of the contact surface. The proposed model and its predicting capabilities are then evaluated against a simplified blade-damper model, based on an underplatform damper test rig recently developed by the authors. A semi-analytical contact solver is used to tune the parameters of the contact element starting from the profilometer measurements of the real damper surface. A comparison with a more simplistic modelling approach based on macroslip contact elements, highlights the improved accuracy of the new model to predict the experimental nonlinear response, when information about the surface roughness is available.

Keywords: Microslip model, damper model, friction damping, turbine blade vibrations, nonlinear dynamics, bladed disks

1. Introduction

One of the most common causes of failure for gas turbines is high-cycle fatigue (HCF) driven by large resonant stresses [1]. Underplatform dampers are devices used by aeroengine manufacturers to reduce the risk of HCF failure, since they dissipate the vibrational energy while at the same time acting as a seal between blades to increase the thermodynamic efficiency [2, 3]. Due to the nonlinear nature of the contact forces, characterised by stick-slip and separation, the dynamic behaviour of the blades becomes very nonlinear making its analysis much more complex. Continuous research has been conducted in this field for the development of new numerical damper models which attempted to improve the fidelity and/or computational cost [4–7]. Most of the modelling approaches proposed rely on frequency domain solvers based on the multi-harmonic balance method in conjunction with continuation techniques, as they represent an efficient approach when only the steady-state response is of interest [8–10].

Various contact models have been used to simulate the interaction between the platform and the blades, which can be classified as macroslip models [11–14] or microslip models [3, 15, 16]. The microslip models are characterised by a smooth and progressive transition between an elastic contact and a sliding one, as opposed to the sharp transition

*Corresponding author.
E-mail address : luca.pesaresi12@imperial.ac.uk.
Tel.: +44 (0)207 594 2117

of the macroslip models. Initially, the macroslip contact models were only 1D [11], and were extended subsequently to allow relative normal motion between the damper and platform [5, 12, 14]. In [13], a fully coupled 3D macroslip contact model, capable of simulating a coupled in-plane 2D motion and the normal relative motion was developed. With regards to the microslip models, various concepts have been developed [15–17] with the most common being a parallel elasto-plastic springs arrangement, initially proposed by Iwan in [18] for 1D tangential motion, and then recently extended to allow relative normal motion in [19, 20].

When a microslip contact model is employed, a single element can be used to describe the behaviour of the whole contact interface and specifically-designed experimental set-ups are used to tune the element [3, 21, 22]. This approach works well for non-conforming contact surfaces (cylindrical dampers), since the contact is normally very localised. However, it could lead to an over-simplification for conforming contacts (wedge dampers) since the kinematics of the contact, which is partially lost using one single microslip element, plays a significant role on the nonlinear dynamic behaviour [23]. To better capture the local kinematics, a small number of microslip elements has also been used [24], which however raises some issues on how the calibration of each contact element should be performed.

A rather different approach to model microslip, which allows an improved description of the contact kinematics, is to discretise the contact area with a dense grid of macroslip contact elements [6, 7, 25, 26]. When this approach is chosen, a significant microslip behaviour can be observed only when a pressure gradient is present at the contact interface as shown in [25]. However, in real contacts, frictional dissipation can also occur with a nominally uniform pressure distribution, since on the scale of the asperities, no contact is truly conforming due to the surface roughness [27]. For this reason, the overall microslip behaviour observed could be seen as the combination of two microslip processes with different scales, a larger scale microslip due to non-uniform pressure distribution, and the microscale microslip at the asperity level. This assumption still constitutes a simplification, as real surfaces can have different levels of roughness at different scales, and are sometimes described using fractals within the contact mechanics community [28].

In this study a new modelling approach for the nonlinear dynamics of blade-damper systems is presented, which aims at being predictive by exploiting information about the contact interface. The proposed approach is characterised through the discretisation of the contact area with a dense grid of microslip contact elements, which are tuned to reproduce the macroscale contact properties, as well as the micromechanical properties due to roughness. For this scope, a new 3D microslip contact model based on a modified Valanis elasto-plastic model [29, 30] is used, and it is then tuned numerically using a semi-analytical contact solver [31]. The modelling approach is then evaluated against an underplatform damper test rig recently developed by the authors [25, 32], showing some promising capabilities for the prediction of the nonlinear dynamics of the blades.

2. Modelling approach

The modelling approach proposed in this paper is based on the previous work presented in [4, 25], but introduces a new contact element and a new tuning procedure which attempts to increase the fidelity of the contact description at the platform-damper interface. Although the main focus of this work is on the modelling of wedge dampers, the same approach could be also applied to other structures which have friction nonlinearities caused by conforming contacts. The damper is included in the model explicitly, using an FE description which allows to account for its flexibility and inertia properties. This aspect is important for dampers which are relatively flexible and that operate close to a "stuck" condition, since neglecting the local flexibility might lead to inaccuracies in the calculation of the contact forces. A damper operates close to a "stuck" condition when microslip is the main dissipation mechanism at the interface, and the damper does not enter a gross sliding regime.

The damper and the blades FE models are then coupled using a series of newly-developed contact elements, which are described in details in the next section. To allow an accurate description of the contact properties, the damper-platform interface is discretised with a grid of contact elements, each of those representing the contact behaviour of a portion of the contact as shown in Fig.1. Due to the manufacturing tolerances, even nominally conforming surfaces can be characterised by a lack of conformity which, together with non-uniform normal loading might lead to a non-uniform pressure distribution as shown in the example of Fig.1. This variation of pressure is taken into account by explicitly defining a different initial pre-load on each element depending on its position on the contact interface, and on the area of the associated patch. At the same time, the micro-mechanical behaviour due to the surface roughness is implicitly taken into account in the model by the new contact elements, using a calibration procedure described

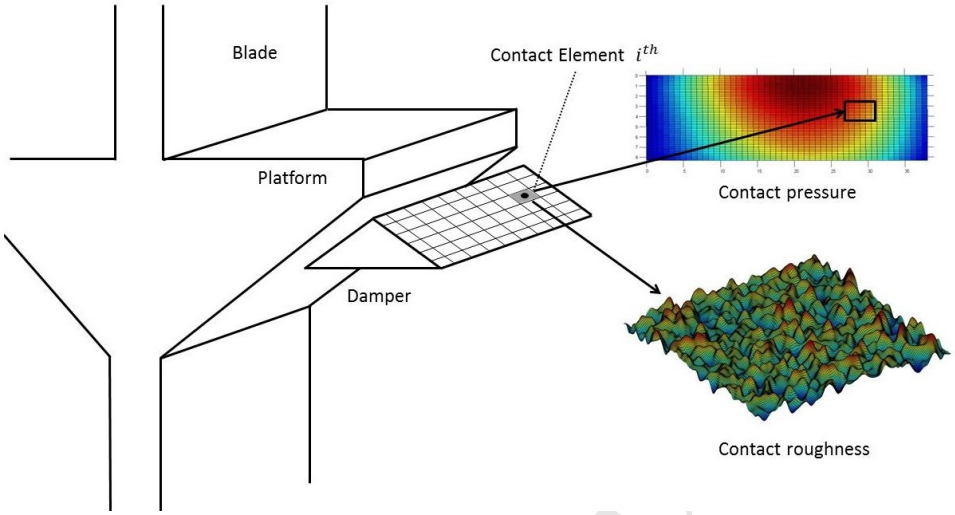

Figure 1: General idea of the two-scales contact interface discretisation.

in section 5. This approach allows the effect of surface roughness to be included in the dynamic model at a low computational cost. In fact, the alternative of explicitly including roughness in the dynamic model would require a much finer mesh (different order of magnitude), which would result in a model more computationally expensive to run.

The dynamic analysis is based on an existing multi-harmonic balance (MHBM) solver with continuation coupled with a model reduction technique, included in the code FORSE (FOrced Response SuitE) and discussed in detail in [4, 14, 33]. Due to the friction forces arising at the contact interface, the equations of motion for the blades and damper are nonlinear, and can be written in the following form:

$$\mathbf{M}\ddot{\mathbf{x}}(t) + \mathbf{C}\dot{\mathbf{x}}(t) + \mathbf{K}\mathbf{x}(t) + \mathbf{F}_{nl}(\dot{\mathbf{x}}(t), \mathbf{x}(t)) = \mathbf{P}(t). \tag{1}$$

where $\mathbf{M}$, $\mathbf{C}$, $\mathbf{K}$ are the mass, damping, and stiffness matrices. $\mathbf{P}$ are the external excitation forces and $\mathbf{F}_{nl}$ are the nonlinear contact forces dependent on the relative motion of the interacting nodes at the interface. According to the MHBM, the response for each DOF of the system can be expressed as a Fourier series truncated at the n^{th} harmonic:

$$\mathbf{q}(\mathbf{t}) = \mathbf{Q}_0 + \sum_{j=1}^{n} \mathbf{Q}_j^c \cos(m_j \omega t) + \mathbf{Q}_j^s \sin(m_j \omega t) \tag{2}$$

where $\mathbf{Q}_0$, $\mathbf{Q}_j^c$ and $\mathbf{Q}_j^s$ are the harmonic coefficients for each DOFs, and $m_j = 0, 1, 2..n$ is an integer corresponding to the relative harmonic. When equation 2 is inserted in equation 1, and the harmonic terms balanced with a Galerkin projection, a system of equations to determine all harmonic components can be obtained in the frequency domain as follows:

$$\mathbf{Z}(\omega)\mathbf{Q} + \mathbf{F}(\mathbf{Q}) - \mathbf{P} = 0 \tag{3}$$

where $\mathbf{Q} = \{\mathbf{Q}_0, \mathbf{Q}_1^c, \mathbf{Q}_1^s, \ldots, \mathbf{Q}_n^c, \mathbf{Q}_n^s\}^T$ is a vector of harmonic coefficients, $\mathbf{F}(\mathbf{Q})$ is the vector of nonlinear forces and $\mathbf{P}$ is the external excitation. $\mathbf{Z}(\omega)$ is the dynamic stiffness matrix of the system. To reduce the size of the problem, a model reduction based on a FRF matrix representation is applied [33], and the harmonic coefficients are then calculated with a Newton-Raphson iterative solver.

3. 3D Microslip Contact Element

A new microslip contact element, which enables to simulate 3D contact motion while taking into account the microslip effects due to surface roughness was used for the present analysis and implemented in the nonlinear dynamic

code FORSE. This element is based on the Valanis model, originally developed to describe the elasto-plastic behaviour of materials under cyclic loading conditions [29]. The Valanis model was then succesfully employed in [30] to model the frictional hysteretic behaviour of a lap joint subject to harmonic excitation. In the present study, the model was modified to allow the inclusion of a variable time-dependent normal load $F_z(t)$, as originally proposed in [34]. With this approach, the friction limit is time-dependent, allowing a full coupling between the tangential and normal relative displacements at the contact interface. This aspect is particularly important for modelling wedge dampers, as the inclination of the interface relative to the platform causes a significant component of normal motion, which strongly influences the energy dissipation mechanism at the interface. With this modification, the rate of change of the tangential friction force can be written as follows:

$$\dot{F} = E_0 \dot{q}(t) \frac{\left[1 + \frac{\lambda(t)}{E_0} \frac{\dot{q}(t)}{|q(t)|} \left(E_t q(t) - F(t)\right)\right]}{\left[1 + k \frac{\lambda(t)}{E_0} \frac{\dot{q}(t)}{|q(t)|} \left(E_t q(t) - F(t)\right)\right]} = f(q, \dot{q}, F, \lambda) \tag{4}$$

where E_0 corresponds to the tangential contact stiffness of the initial loading, E_t is the slope of the macroslip region, k is a parameter which characterises the microslip transition, q is the contact tangential displacement, and λ is a time-dependent function defined as:

$$\lambda = \frac{E_0}{\mu F_z(t) \left(1 - k \frac{E_t}{E_0}\right)} \tag{5}$$

The differential equation 4 is then solved with a numerical scheme to obtain the value of the force at each time step. One of the advantage of the Valanis formulation is that, by defining a positive value for E_t, it permits to reproduce contact hysteresis loops where the macroslip region has a slope. This contact behaviour has been observed experimentally in friction joints that are subject to fretting wear, as reported in [30, 35].

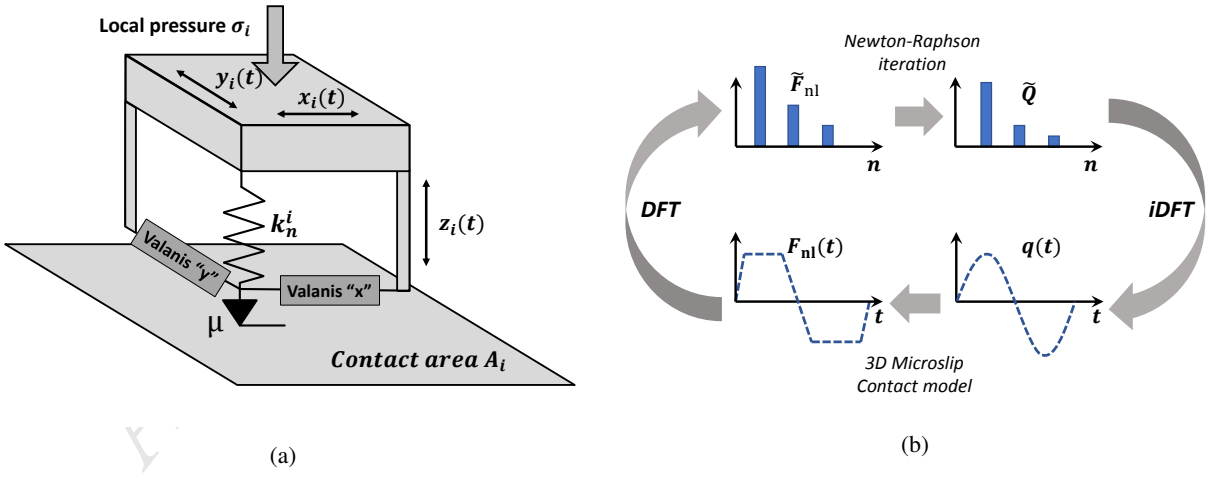

(a) (b)

Figure 2: a) New 3D microslip element schematic, b) general scheme of the alternate frequency-time (AFT) method.

To simulate a full 3D motion, two Valanis elements were used along the x and y direction of the local coordinate system defined for the element "i" as shown in Fig.2a. This allows the description of a 2D in-plane motion, even if there is no coupling between the two directions. For each contact element "i" of the discretised interface, a set of parameters needs to be defined: E_0, E_t, k, the friction coefficient μ, the normal contact stiffness k_n, and the initial element pre-load $N_0 = \sigma_i A_i$, with σ_i and A_i being the local pressure and contact area associated with the element. In this study, a simplification was made assuming the parameters E_0 and k_n constant with time, but the model is flexible to allow the inclusion of different load-dependent stiffness laws for future implementation.

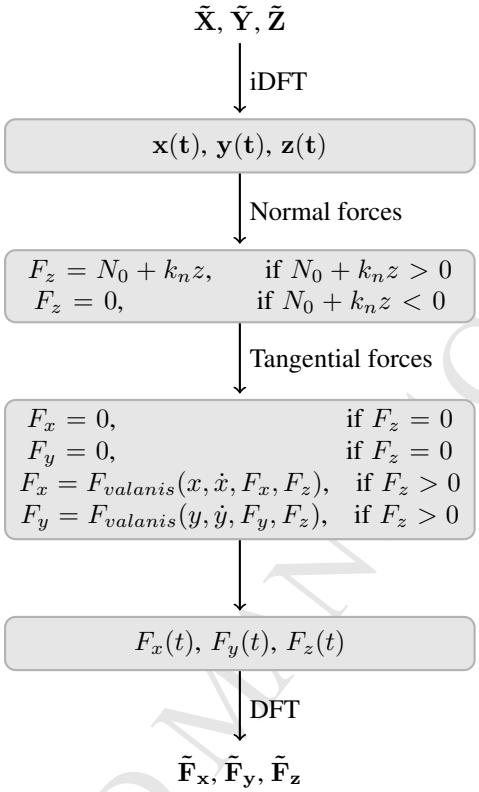

Figure 3: Flow-chart of the contact element routine.

An alternate frequency-time method (AFT) [8] is used to allow an easier calculation of the contact forces which are nonlinear with displacements, using a separate routine in the time-domain as shown in Fig.2b. A simplified flow-chart for the calculation of the contact forces of the 3D microslip element is shown in Fig.3. The contact relative displacements $\tilde{\mathbf{X}}$, $\tilde{\mathbf{Y}}$ and $\tilde{\mathbf{Z}}$ of the mating nodes between the platform and the damper are expressed as harmonic coefficients in the local coordinate system. An inverse Fourier transformation is then applied, and the nonlinear contact forces are then evaluated, using an implicit Euler's method for the tangential forces. The contact forces for the three directions in the local coordinate system are then transformed back to the frequency-domain, $\tilde{\mathbf{F}}_\mathbf{x}$, $\tilde{\mathbf{F}}_\mathbf{y}$, $\tilde{\mathbf{F}}_\mathbf{z}$ and this force calculation is repeated until convergence is reached for the Newton-Raphson scheme. Using the same AFT method, the local tangent matrix of each contact element is calculated with finite difference, and then assembled in the global Jacobian of the system.

Some initial tests on a single contact element were run to evaluate its capability to simulate the contact hysteresis under an oscillating input motion (see Fig.4). The parameter "k", which controls the level of "microslip" in the contact, can vary from "0" (high microslip) to "1" (no microslip), and the effect of this variation under a constant normal load is shown in Fig.4a. Therefore, by changing "k", the smoothness of the microslip transition can be easily controlled, and with a high value its behaviour becomes very similar to a macroslip model (eg. Jenkins).

One of the drawbacks of using the Valanis model for friction contacts, is that unlike in other contact models, the initial loading slope, which corresponds to E_0 (point A in Fig.4a), is different from the "re-loading slope" (point B in Fig.4a). In fact, from equation 4, for $E_t = 0$, the re-loading slope is equal to $2E_0/(1+k)$, and therefore it is always higher than E_0 apart from the limit case $k = 1$, which is not defined. Since only the steady-state solution is of interest here, the initial load is always neglected, and for a correct analysis, the dependence of the contact stiffness on k must be taken into account when specifying the input parameters.

To evaluate the capability of the new contact model under coupling conditions, a tangential harmonic motion coupled to an in-phase normal motion with a separation event is shown in Fig.5. As a result of this coupling, the

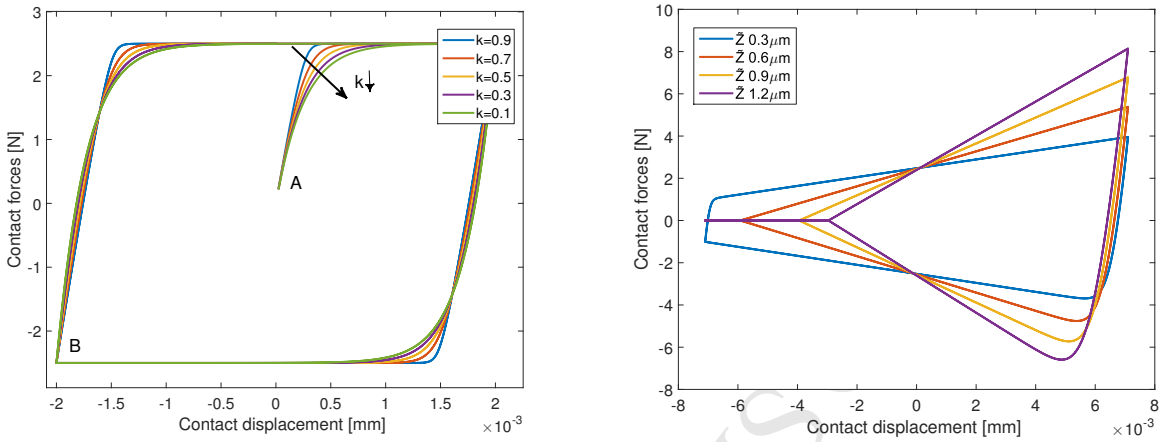

(a) (b)

Figure 4: a) Contact hysteresis loops with varying microslip parameter "k", b) contact hysteresis loops with increasing normal displacement.

tangential friction force is not constant anymore at the sliding limit, but follows the curve $\mu N(t)$. When the amplitude of the normal motion is increased, the contact hysteresis loops are progressively deformed, showing a flat part on the left side which corresponds to the separation event as shown in Fig.4b.

As previously described, the inclusion of the effect of microslip in the contact model should lead to a different energy dissipation at the contact interface compared to a macroslip model (eg. Jenkins). To further investigate this aspect, the energy dissipated per cycle (area of the contact hysteresis loop) was estimated for the new microslip contact model, and then compared to a Jenkins macroslip model at various tangential displacement amplitudes. The results for two different levels of tangential contact stiffness of respectively $E_0 = 10$ kN/mm and $E_0 =$5 kN/mm are shown in Fig.6 for amplitudes up to 0.8 μm, a friction coefficient $\mu = 0.5$ and a constant normal load of 5 N. As shown in Fig.6a, decreasing the value k leads to an increase of energy dissipation compared to the macroslip model. It can also be noted that at higher amplitudes the curves tend to have the same slope, with an inverted order for the dissipated energy (see the small offset in the close up of Fig.6a). Therefore, it should be concluded that at some point in the curve there is a crossing, which tends to be at higher amplitudes for smaller values of k. A lower contact stiffness (see Fig.6b) leads to a wider range where the microslip element is effective in energy dissipation compared to the macroslip one. These results confirm the intuition that the main difference between the two models in terms of energy dissipation appears in the medium/low range of amplitudes, whereas they tend to behave similarly when the contact interface enter the gross slip regime, or when the displacement is near zero.

4. Test case - UPD rig

To validate the proposed modelling approach, an underplatform damper (UPD) rig recently developed at Imperial College London was chosen as the main test case. A full description of the rig is presented in [25, 32], and only a brief presentation is reported here. The UPD rig is an experimental set-up that allows the investigation of the effect of UPDs on blade-like structures under a controlled lab environment. The assembly of the rig can be seen in Fig. 7. During the design, particular care was taken to minimise the imapct of external factors, and focus the study on the nonlinearity introduced by the damper. Two pseudo beam-like blades are fixed to a common base, simulating a rigid disk, and are clamped via a hydraulic cylinder to a large inertia block. The blades and its base were wire cut from a single block in order to move frictional interfaces (potential source of nonlinearity) away from the vibrational stresses of the blade root. The damper studied is a wedge type, [3], which has a triangular cross section with a characteristic angle. Unlike a real high pressure turbine blade, the aerofoil is replaced by a straight rectangular cross-section beam, but still maintaining vibration modes similar to a real blade. The centrifugal load is simulated via a pulley system with calibrated masses, and the excitation is provided by an electrodynamic shaker (Data Physics V4) attached near

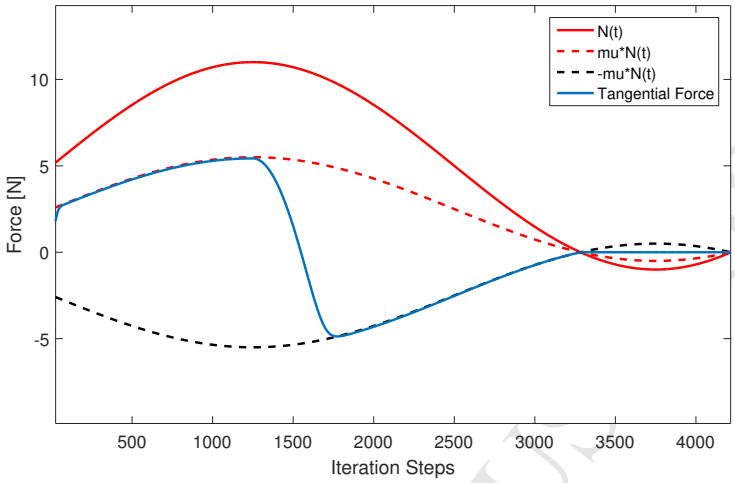

Figure 5: Tangential contact force calculated under varying normal load.

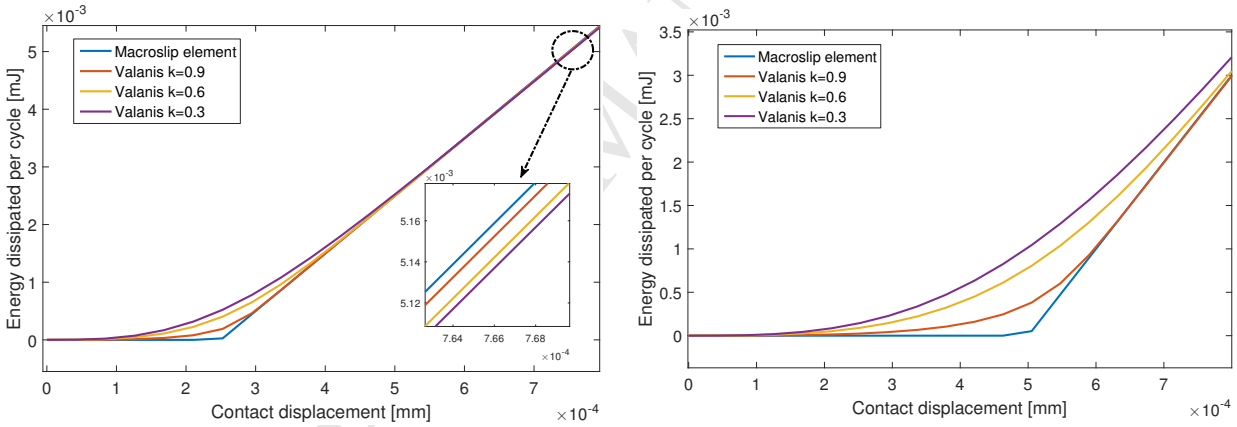

(a) (b)

Figure 6: a) Contact hysteresis dissipated energy $E_0 = 10$ kN/mm, b) contact hysteresis dissipated energy $E_0 = 5$ kN/mm.

the root of the blade to minimise its impact. A non-contact measurement system, which employs two single point laser Doppler vibrometers (Polytec OFV-503) was used to capture the dynamic response of both blades near the tip (see Fig.7). A stepped sine test was performed in a narrow frequency band around the mode of interest, always keeping the excitation force constant within a tolerance range to control the nonlinearity in the system. Different tests were performed with increasing excitation forces in order to progressively activate the friction nonlinearity at the damper-platform interface and characterise the dynamics of the system.

5. Contact element tuning

One of the fundamental steps of the proposed modelling approach is the calibration of the contact parameters for the newly-developed friction contact element. In fact, including more accurate information about the contact interface, which is the driver for the nonlinear behaviour of the system, is very important in improving the prediction capabilities of the proposed modelling approach. The approach proposed here for the contact element tuning is mainly based on a semi-analytical contact solver described in section 5.1, but fully experimental approaches based on specifically-designed test set-ups [35, 36] could be used as well. One of the advantage of a numerical approach is that various

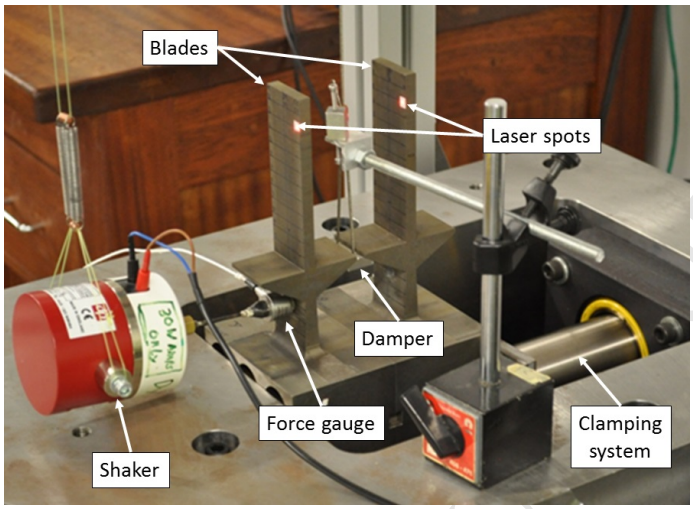

Figure 7: Underplatform damper test rig lab set-up.

rough profiles can be easily investigated, without having to manufacture new specimens with a specific roughness for each new test.

Compared to micro-mechanical rough models, a BEM-based contact solver was used for this study, as it allows the simulation of any rough surface without any assumption on the statistical distribution of the asperities. In addition, this approach allows much faster computations compared to FE rough contact simulations, which normally require prohibitively large models to account for a good representation of the surface features. In the following sections, the contact solver is briefly introduced 5.1, followed by the macroscale tuning of the pressure distribution in section 5.2, and the microscale tuning in section 5.3.

5.1. Semi-analytical contact solver based on the Boundary Element Method (BEM)

A BEM-based contact solver, previously developed by the authors [31, 37, 38], is used here to perform a refined analysis of the damper-platform friction interface and tune the new contact element. The contact solver uses the projected conjugate gradient method [39] and a discrete-convolution fast Fourier transform to accelerate the computation. It assumes the elastic half-space body description, which makes it possible to use the Boussinesq and Cerruti potentials [40, 41] to compute the surface elastic deflections in the normal and tangential directions from the pressures and shear tractions in the contact area. Equation 6 gives the component of normal displacement u_z due to a pressure distribution p. Equation 7 is the discretised form of Eq. 6 on a regular grid of $N_x \times N_y$ points. Similar equations are used to compute the tangential displacements. The first step of the algorithm is to solve the normal contact problem using the conjugate gradient method, after which the tangential problem can be solved using the Coulomb friction law to bound the shear distribution in the slipping region.

$$u_z(x,y) = \frac{1-\nu^2}{\pi E} \int_{-\infty}^{+\infty}\int_{-\infty}^{+\infty} \frac{p(\xi,\eta)}{\sqrt{(\xi-x)^2+(\eta-y)^2}} d\xi d\eta \tag{6}$$

where E and ν are the Young's modulus and Poisson ratio of the material, respectively.

$$u_z(i,j) = K_{zz} \otimes p = \sum_{k=1}^{N_x}\sum_{l=1}^{N_y} p(k,l) K_{zz}(i-k, j-l) \tag{7}$$

where $\otimes$ denotes the discrete convolution product and $K_{zz}(i,j)$ are the discrete influence coefficients [37] that give the normal displacement resulting from unit pressure on the element centred on the grid point (i,j). An extensive validation of the contact solver against standard contact mechanics problems was carried out by the authors in [31].

5.2. Pressure distribution tuning

The pressure distribution at the interface was shown to significantly affect the nonlinear dynamic behaviour of the blade-damper system in [25], and therefore it is important to have an accurate estimation for a predictive model. Initially, a 3D non-contact topography-measuring interferometer Polytec TMS-100 was used to scan both contact surfaces of the damper used, revealing slightly curved profiles (see [25]). However, due to the limited dimensions of the scanning area of the interferometer, it was not possible to measure the surfaces of the platforms. Therefore, this limited the possibility to use the semi-analytical contact solver to obtain the contact pressure distribution, and an experimental approach was preferred instead. Fujifilm prescale pressure films were used at the damper-platform interface, and the prints obtained were then scanned and digitised in MATLAB. A 4^{th} order polynomial was used to approximate the digitised pressure film prints, resulting in a fit with an R-square value of 0.935 (see Fig.8). The obtained pressure distribution was then interpolated to obtain the input pre-loads for each contact element on the interface.

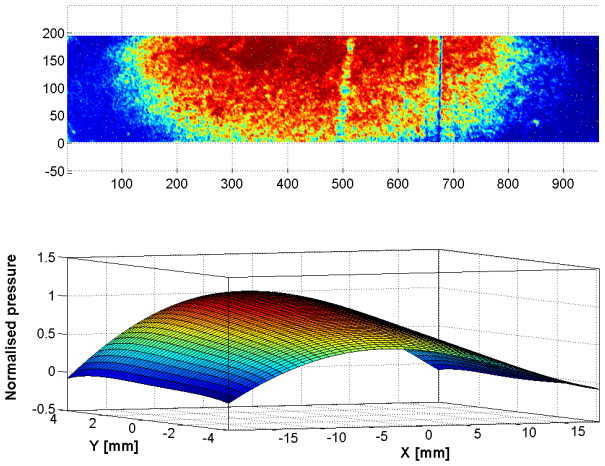

Figure 8: Pressure film digitised and approximated with a polynomial fit.

5.3. Microscale tuning

The semi-analytical contact solver described in section 5.1 was used to numerically tune the newly-developed contact element, allowing the model to reproduce the microslip effects due to the surface roughness, as well as the characteristic stiffness of the contact. Initially, a stylus profilometer was used for both the damper and the platforms showing a Gaussian heights roughness distribution, and an equivalent profile was obtained by subtracting the two. An open source MATLAB tool MySimLabs based on the work of [42] was then used to simulate an equivalent 2D random surface patch with similar roughness to the one measured. An initial uncorrelated random profile Z was generated with an $R_q = 0.177$ μm and then the profile was convoluted using a Gaussian filter $F = e^{(-2(x^2+y^2)/cl^2))}$ as follows:

$$Z_c = \frac{2rl}{\sqrt{\pi}} \frac{cl}{N} * iFFT(FFT(Z) * FFT(F)) \tag{8}$$

where Z_c is the isotropic correlated profile with correlation length cl, patch length rl, $Npoints$ and FFT and $iFFT$ are the direct and inverse 2D fast Fourier transforms. The generated patch of 250 μm by 250 μm with $R_q = 0.177$ μm and a correlation length $cl = 6.6$ μm is shown in Fig.9a. A contact mesh of 1024 by 1024 elements was used for the contact simulations, as it allowed a good discretisation of the surface asperities, while keeping an acceptable computational time.

An initial simulation was performed under load-control and assuming a rough elastic contact, in order to obtain the values of the normal contact stiffness k_n for different pressure levels, as shown in Fig.9b. The data were obtained

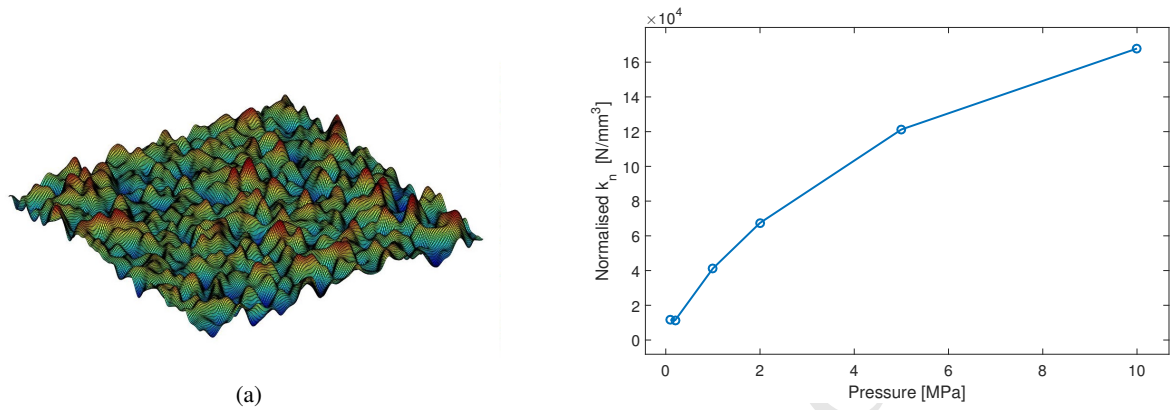

(a) (b)

Figure 9: a) Simulated rough contact patch, b) variation of the parameter "k_n" with contact pressure.

in a range of pressures between 0 to 10 MPa, since these are the values at the damper-platform interface under the 960 N damper load level used for the experiments and subsequent simulations. For the tangential problem, contact simulations were run imposing a sinusoidal displacement, and the corresponding contact hysteresis loops were obtained for different pressure levels (0.1 MPa, 0.2 MPa, 1 MPa, 2 MPa, 5 MPa, 10 MPa) in the range of interest, as shown in Fig.10.

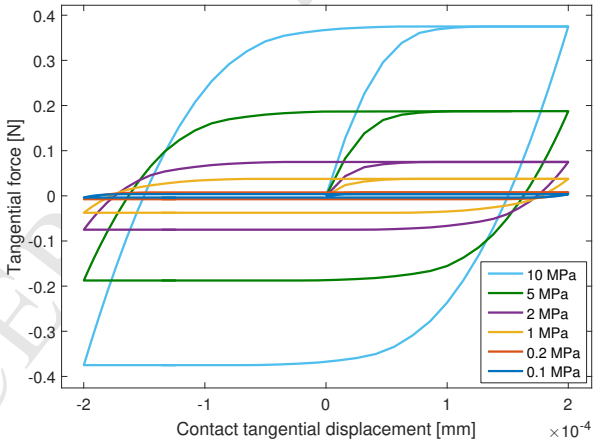

Figure 10: Simulated contact hysteresis loops at different pressure levels.

The friction Coulomb limit was set to be $\mu = 0.6$, since this was the average value measured for the same material in previous experimental tests with a 1D friction rig developed at Imperial College London [43]. The hysteresis loops of Fig.10 were then used to tune the contact element input parameters E_0 and k. Since both E_0 and k influence the stiffness of the contact and its microslip transition, their selection is not trivial, and an optimisation was run in MATLAB based on the interior-point algorithm described in [44]. A set of parameters E_0 and k could be found for each pressure level, which allowed the model to perfectly capture the numerical hysteresis loops. By interpolating the plots of k_n, E_0 and k versus pressure (see Fig.9b, Fig.11a and Fig.11b), it was possible to specify a set of optimised parameters for each contact element at the damper-platform depending on the element pre-load (which comes from the pressure films). A monotonic increasing trend was obtained for k_n and E_0, which indicates the tendency of the normal and tangential stiffness to increase at higher pressure, whereas a more complex behaviour characterised by a minimum close to 1 MPa was obtained for the microslip parameter k. The most significant advantage of the

proposed approach is that the complex micro-mechanical behaviour of the asperities is retained in the model using this calibration process, without having to directly include roughness in the contact mesh.

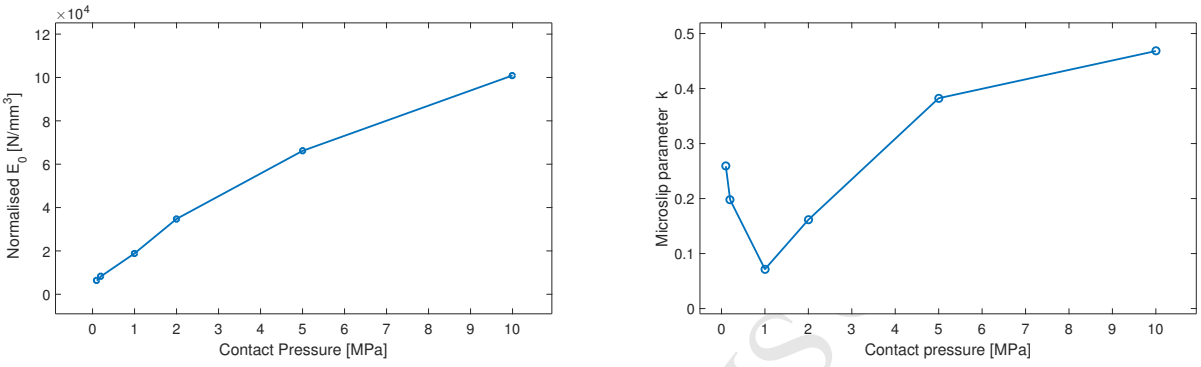

(a) (b)

Figure 11: a) Variation of the parameter "E_0" with contact pressure, b) variation of the microslip parameter "k" with contact pressure.

6. Results and Discussion

In this section, the prediction capabilities of the newly-proposed modelling approach are evaluated against the experimental data of the UPD rig (see section 4), and are compared to the previous model presented in [25]. In the previous modelling approach in [25], macroslip Jenkins elements were used to model the contact interface, and the microscale tuning described in 5.3 was not carried out. Only the macroscale tuning was performed by interpolating the pressure films for a more realistic pressure distribution similarly to here (see section5.2). Therefore, the difference obtained with the previous model allows the evaluation of the contribution of the newly-developed contact element, as well as the tuning procedure described in section 5.3 for a higher fidelity description of the contact properties. In fact, in the previous model [25], the contact stiffness was assumed uniformly distributed with a value of 60000 N/mm^3 for all the contact elements, based on average measurements performed on the 1D friction rig described in [43].

To allow a reliable comparison with the previous results, the finite element models of the blades and damper were kept the same as in [25] (see Fig.12a), as well as the subset of contact nodes used to discretise the damper-platform interface (see Fig.12b). In fact, the size of the nonlinear problem to solve is proportional to the number of contact nodes, and for this reason only 146 node-to-node pairs were included in the model to significantly reduce the computational cost. This reduction is performed by superimposing a triangular 2D mesh to the original contact FE mesh, and only the FE mesh nodes closest to the centroids of the new triangles are selected. For a more accurate reduction, the contact element parameters, which are normalised by the area (pressure, k_n, E_0), are then scaled proportionally to the area of the associated triangle of the new mesh.

The mode investigated for the present study is the first flexural out-of-phase (OOP) mode shown in Fig.12a, where the two blades move against each other. This mode was chosen because the damper operates close to a "stuck" condition with some microslip, whereas the in-phase mode is dominated by large separation at the contact interface (see [23]), and it is therefore much less interesting for the evaluation of the new approach. To ensure an accurate starting point for the nonlinear analysis, some initial experiments were performed without the damper, in order to update the FE linear model and evaluate the background damping caused by the material and set-up configuration including the shaker. A stepped sine shaker test was performed around the first flexural mode (see Fig.13), and a manual FE model update led to an estimated first resonance of 269.7 Hz, which is very close (0.07% lower) to the measured 269.9 Hz mode shown in Fig.13a. To estimate the experimental frequency and damping, the measured FRF was fitted using an implementation of the poly-reference Least Squares Complex Frequency algorithm (pLSCF) [45], as shown in Fig.13. A loss factor of $\eta = 0.04\%$ was extracted and it was included as modal damping in the linear model.

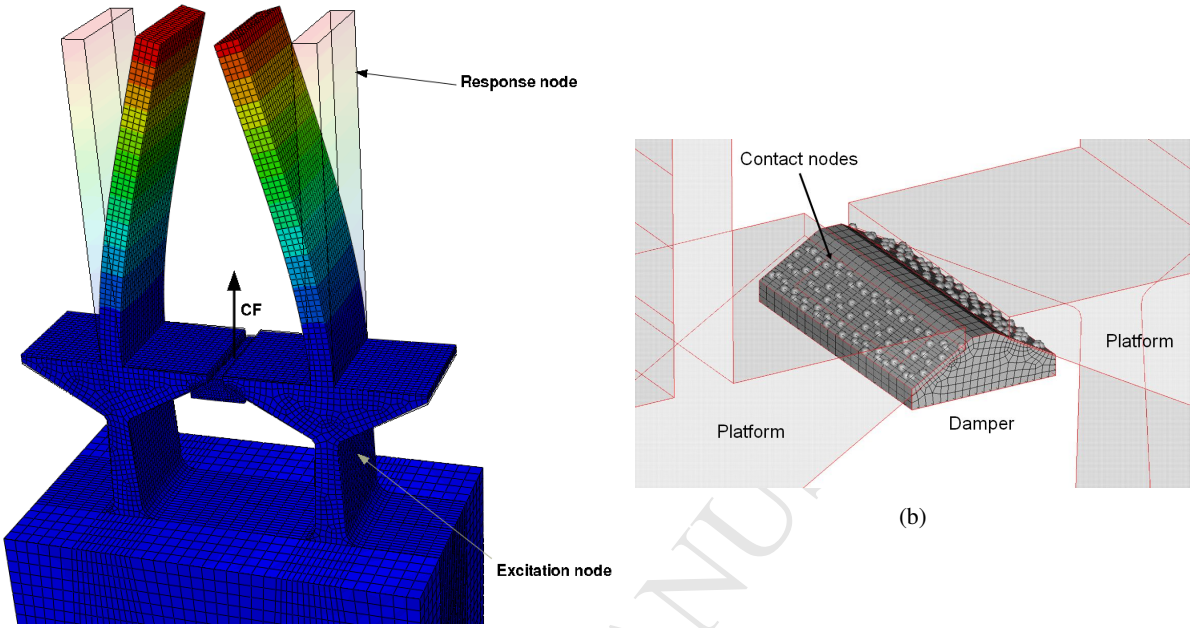

(a) (b)

Figure 12: a) First flexural OOP mode of the blades and damper, b) contact friction elements at the damper-platform interface.

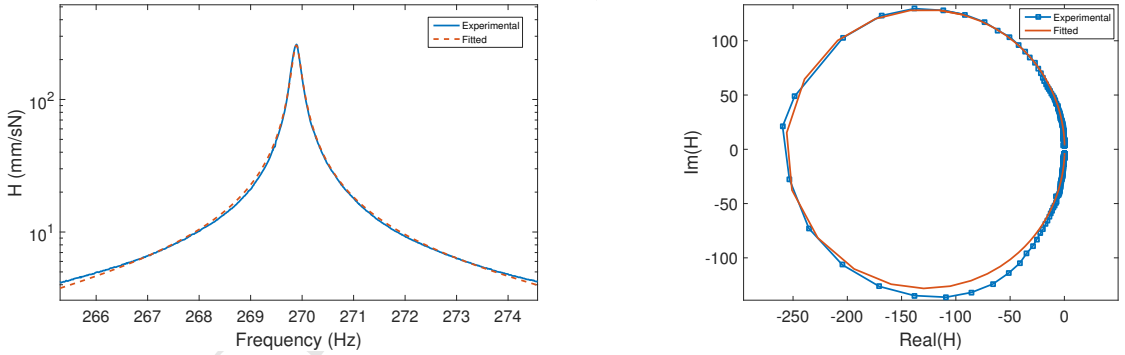

(a) (b)

Figure 13: First flexural mode without damper: a) experimental and fitted linear FRF amplitude, b) experimental and fitted Nyquist plot.

The nonlinear measurements with the damper in place were performed using a constant damper load of 960 N, which allowed a good conformity at the contact interface. A higher uncertainty in the repeatability of the FRFs was found at lower damper loads, and for this reason this regime was avoided for the present validation. Force-controlled shaker tests were conducted starting from 0.096 N up to 17 N (shaker limit) to gradually activate the frictional contact nonlinearity. The nonlinear FRFs of the experiments, new modelling approach, and old modelling approach are all compared in Fig.14, and the excitation and response locations can be seen in Fig.12a.

Thanks to an improved description of the stiffness distribution at the contact interface, the resonance frequency of the nearly-linear excitation case for the new model is slightly closer to the experiments, being 0.92% higher compared to the 1.01% of the previous model. Both models tend to overestimate the resonance frequency of the experimental OOP mode, which lies at 435.8 Hz. A possible explanation for this behaviour could be an overestimation of the contact area in the model caused by the uncertainty in the polynomial approximation of the experimental pressure films. With

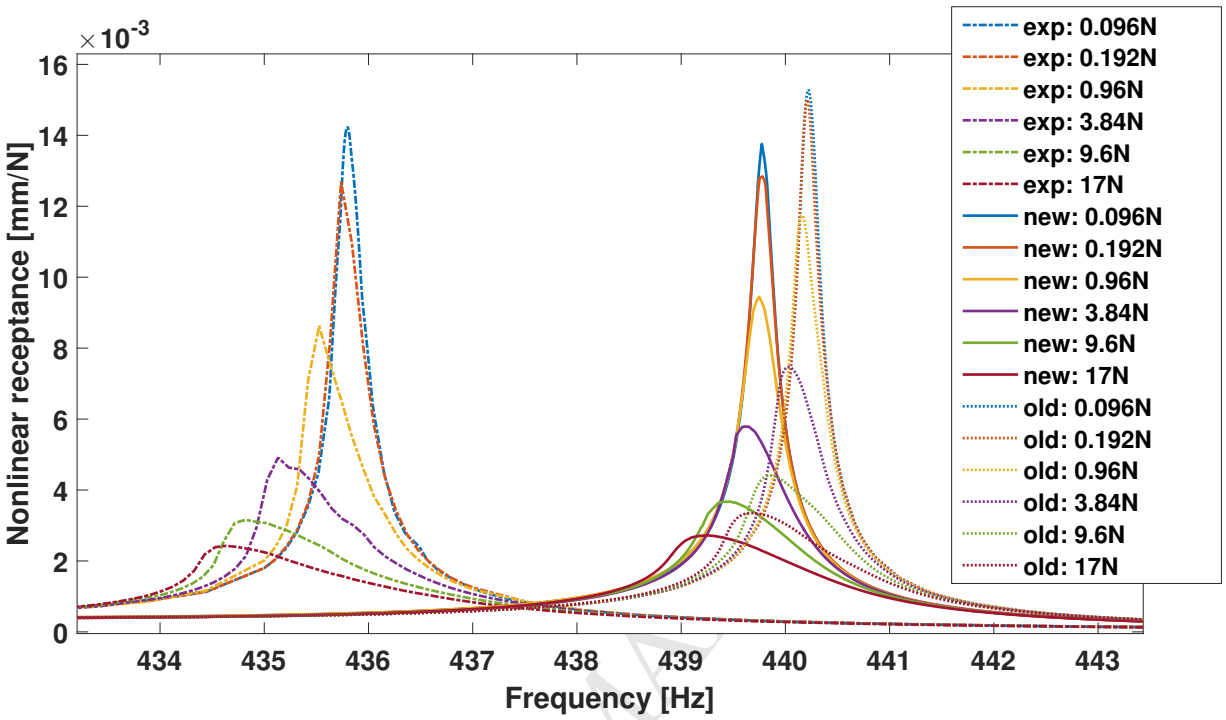

Figure 14: Nonlinear FRFs at increasing excitation levels.

regards to the amplitude estimation, the new model significantly improves the prediction accuracy compared to the previous model. In Fig.15a, the nonlinear peak FRFs of the experiments and the two models are compared for the various excitation levels. Both models can capture the decreasing trend, but the new approach is much closer to the experimental curves, having an average amplitude percentage difference of 9.9%, compared to an average 31.9% of the previous model. A comparison of the prediction errors between the two models for each excitation level is shown in Fig.15b. The new approach significantly improves the amplitude predictions at all excitation levels, with a particularly good agreement with the measurements in the lower range of excitations.

Therefore, taking into account the micromechanical contact properties, including microscale miscroslip dissipation and stiffness distribution due to surface roughness, a significantly improved amplitude estimation was achieved. These results highlight the promising capabilities of the new modelling approach for accurate dynamic predictions. The slight overestimation of the experimental nonlinear amplitudes observed is still acceptable, since factors such as the additional damping which might have been introduced by the damper pulling wire, were not included in model. More investigations need to be performed for an improved evaluation of the damper-platform contact area, since this is one of the main factors for an accurate prediction of the resonance frequencies of the system when the damper is in place. Other extensions of the work could evaluate the inclusion of roughness evolution due to contact wear, using an approach on the microscale similar to the one used for the macroscale in the study by Armand et al. [37].

7. Conclusions

In this study, a new modelling approach for underplatform dampers was presented and evaluated against the experimental data of a recently-developed test rig. The new model employs a dense discretisation of the damper-platform interface with a grid of 3D microslip contact elements. For this scope, a new 3D contact element based on a modified Valanis model was developed, and preliminary tests highlighted its capabilities for representing significant contact nonlinearities including contact separation. The key idea of the proposed approach is to include the micromechanical contact behaviour in the model by using an appropriate tuning procedure for each contact element. In particular the

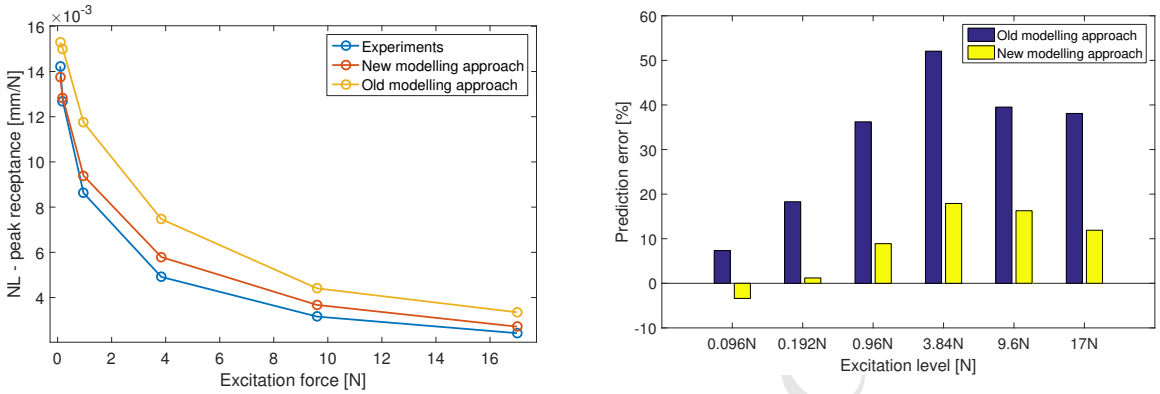

(a) (b)

Figure 15: a) Comparison of peak nonlinear amplitudes at increasing excitation levels, b) amplitude prediction error comparison.

new model is able to capture both the contribution of a macroscale microslip, due to non-uniform pressure distribution, as well as the microscale microslip due to the surface roughness. A numerical tuning procedure for the microslip elements is also proposed, based on the simulations of the normal and tangential behaviour of a representative contact patch having similar roughness characteristics to the real contact. For this purpose, a BEM-based contact solver developed by the authors was used, which allows the simulation of any kind of contact surface, including non-isotropic and non-Gaussian ones.

The new modelling approach proved to be very effective in capturing the amplitude levels of the nonlinear FRFs, leading to a significant improvement compared to the previous models based on the use of macroslip contact elements. These findings suggest the relevance of the microscale dissipation, as well as of the improved description of the contact stiffness distribution, in the overall frictional dissipation mechanism at the contact interface. In addition, the proposed modelling approach only relies on the measurement of some contact properties, such as the contact pressure, roughness and friction coefficient, and therefore it represents a promising tool for the prediction of the nonlinear dynamic behaviour of blades constrained by friction dampers. Moreover, the flexibility of the modelling approach proposed allows it to be extended to other types of mechanical structures with other types of frictional contacts.

Acknowledgments

The authors are grateful to Innovate UK and Rolls-Royce plc for providing the financial support for this work and for giving permission to publish it. This work is part of a collaborative R&T project SILOET II P19.6 which is co-funded by Innovate UK and Rolls-Royce plc and carried out by Rolls-Royce plc and the Vibration UTC at Imperial College London.

References

[1] B.A.Cowles, High cycle fatigue in aircraft gas turbine - an industry prospective, International Journal of Fracture 80 (1996) 147–163. doi:10.1007/BF00012667.

[2] J. H. Griffin, A review of friction damping of turbine blade vibration, International Journal of Turbo and Jet Engines 7 (1990) 297–307.

[3] K. Y. Sanliturk, D. J. Ewins, A. B. Stanbridge, Underplatform Dampers for Turbine Blades: Theoretical Modeling, Analysis, and Comparison With Experimental Data, Journal of Engineering for Gas Turbines and Power 123 (4) (2001) 919. doi:10.1115/1.1385830.

[4] E. P. Petrov, Explicit Finite Element Models of Friction Dampers in Forced Response Analysis of Bladed Disks, Journal of Engineering for Gas Turbines and Power 130 (2) (2008) 022502. doi:10.1115/1.2772633.

[5] C. M. Firrone, S. Zucca, M. M. Gola, The effect of underplatform dampers on the forced response of bladed disks by a coupled static/dynamic harmonic balance method, International Journal of Non-Linear Mechanics 46 (2) (2011) 363–375. doi:10.1016/j.ijnonlinmec.2010.10.001.

[6] E. Cigeroglu, N. An, C. H. Menq, Forced Response Prediction of Constrained and Unconstrained Structures Coupled Through Frictional Contacts, Journal of Engineering for Gas Turbines and Power 131 (2) (2008) 919. doi:10.1115/1.2940356.

[7] L. Panning, W. Sextro, K. Popp, Spatial Dynamics of Tuned and Mistuned Bladed Disks with Cylindrical and Wedge-Shaped Friction Dampers, International Journal of Rotating Machinery 9 (2003) 219–228. doi:10.1155/S1023621X03000198.

[8] M. Krack, L. Salles, F. Thouverez, Vibration prediction of bladed disks coupled by friction joints, Archives of Computational Methods in Engineering (2016) 1–48doi:10.1007/s11831-016-9183-2.

[9] M. Krack, L. Panning, J. Wallaschek, A high-order harmonic balance method for systems with distinct states, Journal of Sound and Vibration 332 (21) (2013) 5476 – 5488. doi:doi:10.1016/j.jsv.2013.04.048.

[10] L. Salles, B. Staples, N. Hoffmann, C. W. Schwingshackl, Continuation techniques for analysis of whole aeroengine dynamics with imperfect bifurcations and isolated solutions, Nonlinear Dynamics 86 (3) (2016) 1897–1911. doi:10.1007/s11071-016-3003-y.

[11] J. H. Griffin, Friction Damping of Resonant Stresses in Gas Turbine Engine Airfoils, Journal of Engineering for Power 102 (1980) 329–333.

[12] B. D. Yang, C. H. Menq, Characterization of Contact Kinematics and Application to the Design of Wedge Dampers in Turbomachinery Blading : Part 1 — Stick-Slip Contact Kinematics, Journal of Engineering for Gas Turbines and Power 120 (1998) 410–417. doi:10.1115/1.2818138.

[13] B. Yang, C. Menq, Characterization of 3d contact kinematics and prediction of resonant response of structures having 3d frictional constraint, Journal of Sound and Vibration 217 (5) (1998) 909 – 925. doi:http://dx.doi.org/10.1006/jsvi.1998.1802.

[14] E. P. Petrov, D. J. Ewins, Analytical Formulation of Friction Interface Elements for Analysis of Nonlinear Multi-Harmonic Vibrations of Bladed Disks, Journal of Turbomachinery 125 (2) (2003) 364. doi:10.1115/1.1539868.

[15] C. H. Menq, J. Bielak, J. Griffin, The influence of microslip on vibratory response, part I: A new microslip model, Journal of Sound and Vibration 107 (2) (1986) 279–293. doi:10.1016/0022-460X(86)90238-5.

[16] G. Csaba, Forced Response Analysis in Time and Frequency Domains of a Tuned Bladed Disk With Friction Dampers, Journal of Sound and Vibration 214 (3) (1998) 395–412. doi:10.1006/jsvi.1997.1513.

[17] K. Sanliturk, D. J. Ewins, Modelling Two-Dimensional Friction Contact And Its Application Using Harmonic Balance Method, Journal of Sound and Vibration 193 (1996) 511–523. doi:10.1006/jsvi.1996.0299.

[18] W. D. Iwan, A distributed-element model for hysteresis and its steady-state dynamic response, Journal of Applied Mechanics 33 (4) (1966) 893–900. doi:10.1115/1.3625199.

[19] M. Rajaei, H. Ahmadian, Development of generalized Iwan model to simulate frictional contacts with variable normal loads, Applied Mathematical Modelling 38 (15) (2014) 4006 – 4018. doi:10.1016/j.apm.2014.01.008.

[20] C. Gastaldi, M. M. Gola, An Improved Microslip Model for Variable Normal Loads, Springer International Publishing, Cham, 2015, pp. 169–179. doi:10.1007/978-3-319-06590-8_14.

[21] G. Csaba, Modelling of a microslip friction damper subjected to translation and rotation, in: Proceedings of ASME Gas Turbine and Aeroengine Congress and Exhibition, Vol. 4, 1999, p. V004T03A012.

[22] C. Gastaldi, M. M. Gola, On the relevance of a microslip contact model for under-platform dampers, International Journal of Mechanical Sciences 115–116 (2016) 145 – 156. doi:10.1016/j.ijmecsci.2016.06.015.

[23] L. Pesaresi, M. Stender, V. Ruffini, C. W. Schwingshackl, DIC Measurement of the Kinematics of a Friction Damper for Turbine Applications, Springer International Publishing, Cham, 2017, pp. 93–101. doi:10.1007/978-3-319-54930-9_9.

[24] R. Lacayo, L. Pesaresi, J. Gross, D. Fochler, J. Armand, L. Salles, C. Schwingshackl, M. Allen, M. Brake, Nonlinear modeling of structures with bolted joints: A comparison of two approaches based on a time-domain and frequency-domain solver, Mechanical Systems and Signal Processing 114 (2019) 413 – 438. doi:10.1016/j.ymssp.2018.05.033.

[25] L. Pesaresi, L. Salles, A. Jones, J. Green, C. Schwingshackl, Modelling the nonlinear behaviour of an underplatform damper test rig for turbine applications, Mechanical Systems and Signal Processing 85 (2017) 662 – 679. doi:10.1016/j.ymssp.2016.09.007.

[26] C. M. Firrone, S. Zucca, Modelling friction contacts in structural dynamics and its application to turbine bladed disks, in: J.Awrejcewicz, Numerical Analysis - Theory and Application, INTECH 2011, 2011, pp. 301–334.

[27] C. Putignano, M. Ciavarella, J. Barber, Frictional energy dissipation in contact of nominally flat rough surfaces under harmonically varying loads, Journal of the Mechanics and Physics of Solids 59 (12) (2011) 2442 – 2454. doi:10.1016/j.jmps.2011.09.005.

[28] V. A. Yastrebov, G. Anciaux, J.-F. Molinari, From infinitesimal to full contact between rough surfaces: Evolution of the contact area, International Journal of Solids and Structures 52 (2015) 83 – 102. doi:10.1016/j.ijsolstr.2014.09.019.

[29] K. C. Valanis, Fundamental consequences of a new intrinsic time measure. plasticity as a limit of the endochronic theory, Arch. Mech. 32 (1980) 171 – 191.

[30] L. Gaul, J. Lenz, Nonlinear dynamics of structures assembled by bolted joints, Acta Mechanica 125 (1) (1997) 169–181. doi:10.1007/BF01177306.

[31] J. Armand, L. Salles, C. W. Schwingshackl, Numerical simulation of partial slip contact using a semi-analytical method, in: ASME 2015 International Design Engineering Technical Conferences and Computers and Information in Engineering Conference, American Society of Mechanical Engineers, 2015, pp. V008T13A022–V008T13A022. doi:10.1115/DETC2015-46464.

[32] L. Pesaresi, L. Salles, R. Elliot, A. Jones, J. S. Green, C. W. Schwingshackl, Numerical and experimental investigation of an underplatform damper test rig, Applied Mechanics and Materials 849 (2016) 1–12. doi:10.4028/www.scientific.net/AMM.849.1.

[33] E. P. Petrov, A High-Accuracy Model Reduction for Analysis of Nonlinear Vibrations in Structures With Contact Interfaces, Journal of Engineering for Gas Turbines and Power 133 (10) (2011) 102503. doi:10.1115/1.4002810.

[34] F. Pourahmadian, H. Ahmadian, H. Jalali, Modeling and identification of frictional forces at a contact interface experiencing micro-vibro-impacts, Journal of Sound and Vibration 331 (12) (2012) 2874 – 2886. doi:10.1016/j.jsv.2012.01.032.

[35] C. W. Schwingshackl, E. P. Petrov, D. J. Ewins, Measured and estimated friction interface parameters in a nonlinear dynamic analysis, Mechanical Systems and Signal Processing 28 (2012) 574–584. doi:10.1016/j.ymssp.2011.10.005.

[36] D. Botto, M. Lavella, M. M. Gola, Test Rig for Extraction of the Contact Parameters for Plane on Plane Contact, Proceedings of ASME IDETCdoi:10.1115/DETC2012-709501.

[37] J. Armand, L. Pesaresi, L. Salles, C. Schwingshackl, A Multiscale Approach for Nonlinear Dynamic Response Predictions With Fretting Wear, Journal of Engineering for Gas Turbines and Power 139 (2). doi:10.1115/1.4034344.

[38] J. Armand, L. Salles, C. Schwingshackl, D. S, K. Willner, On the effects of roughness on the nonlinear dynamics of a bolted joint: A

multiscale analysis, European Journal of Mechanics - A/Solids 70 (2018) 44 – 57. doi:10.1016/j.euromechsol.2018.01.005.
[39] I. A. Polonsky, L. M. Keer, Fast methods for solving rough contact problems: A comparative study, J. Tribol. 122 (1) (2000) 36. doi:10.1115/1.555326.
[40] K. L. Johnson, Contact Mechanics, Cambridge University Press, 1985, cambridge Books Online.
[41] A. E. H. Love, A Treatise on the Mathematical Theory of Elasticity, A Treatise on the Mathematical Theory of Elasticity, at the University Press, 1906.
[42] N. Garcia, E. Stoll, Monte carlo calculation for electromagnetic-wave scattering from random rough surfaces, Physical review letters 52 (1984) 1798 – 1801. doi:10.1109/8.560342.
[43] C. W. Schwingshackl, Measurement of Friction Contact Parameters for Nonlinear Dynamic Analysis, in: Proceedings of the Society for Experimental Mechanics IMAC Conference, 2012.
[44] R. H. Byrd, J. C. Gilbert, J. Nocedal, A trust region method based on interior point techniques for nonlinear programming, Mathematical Programming 89 (1) (2000) 149–185. doi:10.1007/PL00011391.
[45] V. Ruffini, T. Nauman, C. W. Schwingshackl, Impulse Excitation of Piezoelectric Patch Actuators for Modal Analysis, Springer International Publishing, 2017, pp. 97–106. doi:10.1007/978-3-319-54810-4_11.